CRITICAL STATE FLOW RULES FOR CFD SIMULATIONS OF WET GRANULAR FLOWS

R. SCHWARZE[1], A. GLADKYY[2] AND S. LUDING[3]

[1] Institute of Mechanics and Fluid Dynamics (IMFD), TU Bergakademie Freiberg,
Lampadiusstr. 2, 09596 Freiberg, Germany
e-mail: ruediger.schwarze@imfd.tu-freiberg.de, http://tu-freiberg.de/fakult4/imfd/mgf/

[2] Institute of Mechanics and Fluid Dynamics (IMFD), TU Bergakademie Freiberg
Lampadiusstr. 2, 09596 Freiberg, Germany
e-mail: anton.gladkyy@imfd.tu-freiberg.de, http://tu-freiberg.de/fakult4/imfd/mgf/

[3] Multi Scale Mechanics (MSM), Engineering Technology (CTW), UTwente
P.O.Box 217, 7500 AE Enschede, The Netherlands
e-mail: s.luding@utwente.nl http://http://www.utwente.nl/ctw/msm/

Key words: Granular Material, Rheology, Critical State, DEM, Wet Contact, Liquid Bridge, Micro-Macro Transition

Abstract. First rheological investigation results of weakly wet granular media are presented. The materials have been examined experimentally and numerically in well-defined shear configurations in steady state, in the intermediate flow regime. For the experiments, a Searl-type ring shear cell with rotating inner cylinder and fixed outer cylinder is used. In the numerical particle simulation approach, a split-bottom shear cell is used. Relevant local continuum flow fields (e.g. velocity, stress, shear rates) are determined by micro-macro transition from the simulations data. After the simulations are validated by experiments, e.g. by comparison with the experimentally accessible quantities like shear-torque at the inner wheel, they can give a deeper insight into the microscopic kinematics. The granular media have considerably more "wet contacts" in the shear zone, as for example the location-plot of purely wet bridges, without mechanical contacts suggests. Finally, critical state flow rules concerning the viscosity of wet granular materials are discussed.

1 INTRODUCTION

Wet and dry granular flows [1, 2] play an important role in geotechnical and geophysical context [3], as well as in several technical processes as, for instance, in the production of sand cores for casting by core shooting [4]. In the latter example, weakly wetted granular materials are mixtures of granular matter and few volume-percent of liquid binder.

These granular flows exhibit very different flow rheology, which can be characterized by the dimensionless shear rate $\dot{\gamma}^* = \dot{\gamma}\sqrt{d_P/g}$ [5] or the similarly defined inertial number $I = \dot{\gamma}\,d_P/\sqrt{p/\rho}$ [1]. In the so-called slow, frictional regime for $\dot{\gamma}^* < 0.2$, multibody interactions and long lasting contacts with forces due to a confinement pressure are predominant. On the contrary, short binary collisions between the fast moving particles and inertial forces dominate in the so-called rapid granular flow regime for $\dot{\gamma}^* > 3$. In the intermediate regime, between slow and rapid, both inertial and pressure interactions between particles have to be considered. Adding a small amount of a wetting liquid to the granular materials induces the formation of capillary bridges between the individual granular particles [3, 6]. The dynamics of the granular flow is significantly changed due to the presence of the capillary bridges. While several proposals for flow rules for different types of dry granular flows are available in the literature (see e.g. [2, 6]) there is little known about the dynamic behavior and flow rules of wet granular materials [7].

From the point-of-view of continuum mechanics, both dry and weakly wet granular materials exhibit non-Newtonian flow behavior, where the relations between shear stresses and shear rates, for example, can be expressed by nonlinear functions. Since the presence of small amounts of liquid already changes the rheological behavior of the granular material markedly [8, 9], detailed knowledge of the constitutive equations of these materials is of fundamental importance for the control of the corresponding processes. As an example, the filling flow – even in complex core boxes – could be analyzed by CFD simulations [10] if the proper rheological model of the material would be known.

Unfortunately, the realization of rheometer experiments involving weakly wetted granular materials is complicated and time consuming. Therefore, alternative and more efficient methods for rheological investigations are highly desirable. In this paper, we use the split-bottom ring shear setup of a rheometer [11] for discrete-element method (DEM) simulations of these partly wet granular materials. Similar DEM simulations of wet granular materials have been performed in order to study the micro-mechanics in different applications [12, 13, 14].

Starting from the DEM results, we apply a local micro-macro transition [16, 17, 18] in order to obtain rheological data, e.g. apparent shear viscosities, for weakly wetted granular materials. First results indicate, that the numerically determined informations exhibit similar differences between dry and wet granular materials as in the experiments.

2 PREVIOUS RHEOLOGICAL MEASUREMENTS

Rheological data of weakly wetted granular materials (core shooting materials based on quartz sand F35, with either synthetic resin or sodium silicate as binder) have been recently measured in a Searl-type rotating viscometer [8, 15] with a fixed bottom and outer cylinder wall and a rotating inner cylinder wall, Fig. 1(left). For the measurements, an external pressure p_e much larger than the hydrostatic pressure level in the viscometer gap was superimposed to the weakly wetted granular material by a top-lid in matching ring-shape.
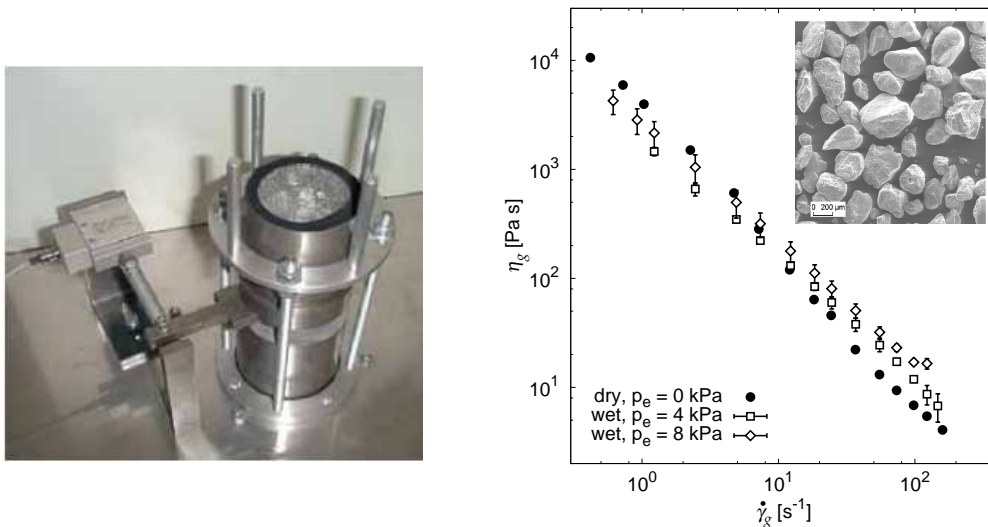
Figure 1: Rheometer measurements, (left) experimental setup (right) apparent shear viscosity η_g as a function of shear rate for a typical core shooting material made of quartz sand F35 (inset: SEM picture of a sample of F35) and two external pressure levels p_e. The solid points represent dry material data, see Ref. [15] for more details.

The apparent (global) shear viscosity

$$\eta_g = \frac{|\tau_g|}{\dot{\gamma}_g} \tag{1}$$

of the core shooting material was found to differ markedly from the values of the dry sand. Here, the quantities τ_g and $\dot{\gamma}_g$ are *globally* defined, i.e. they describe the dynamics of the bulk granular material and set-up: The mean shear stress $\tau_g = F_{t,o}/A_o$ is the quotient of the tangential force $F_{t,o}$ at the outer cylinder wall, and the outer cylinder wall area A_o. The mean shear rate $\dot{\gamma}_g = U_i/b$ is approximated by the quotient of the velocity U_i of the rotating inner cylinder wall and the gap width b.

All measurements indicate shear-thinning behavior of the core-shooting materials, see Fig. 1(right) for an example. The observed apparent shear viscosities $\eta_g (\dot{\gamma}_g)$ follow roughly the same shear-thinning behavior for all investigated core-shooting materials with scaling as $\eta_g \propto \dot{\gamma}_g^{-\alpha}$ with $\alpha \simeq 1$. Additionally, it was found, that the apparent shear viscosity η_g of the core shooting material is smaller than the dry F35 data, but exceeds the dry F35 data markedly for higher shear rates $\dot{\gamma}_g$.

3 MODEL FUNDAMENTALS

The flow of a sheared, weakly wetted granular material is now investigated in more detail by means of DEM simulations. The DEM model is based on Newton's equations of motion for the translational and rotational degrees of freedom of N spherical particle. Here, the inter-particle forces $\underline{f}_{ij}$ are modeled by well-known force-overlap relations

3

in combination with capillary forces, which are induced by liquid bridges between the interacting particles. Details and a validation of our DEM model are given in a recent publication [15], so that they are only briefly touched here.

3.1 Contact force law

The modeling of the contact force is based on the quantities/symbols given in Fig. 2(left). The force $\underline{f}_{ij}$ on particle i, from particle j, at contact c, can be decomposed into a normal and a tangential part as

$$\underline{f}_{ij} = f_{ij}^n \, \hat{n}_{ij} + f_{ij}^t \, \hat{t}_{ij} + f_{ij,c} \, \hat{n}_{ij} \,. \tag{2}$$

with normal $\hat{n}_{ij}$ and tangential unit vector $\hat{t}_{ij}$ at the contact point c. The normal force f_{ij}^n, the tangential force f_{ij}^t and the capillary force $f_{ij,c}$ due to a liquid bridge between particle i and j are specified below.
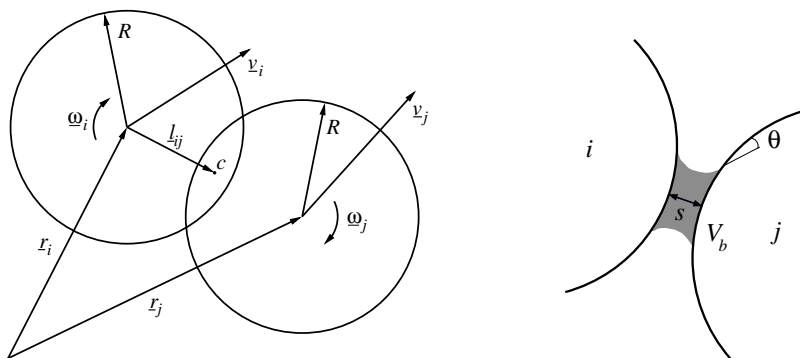
Figure 2: Contact force model based on (left) contact c between two particles i, j and (right) liquid bridge between particles i and j with the bridge length s, the bridge volume V_b and the contact angle θ.

Two dry particles i, j with radius R, which are moving with velocities $\underline{v}_i$ and $\underline{v}_j$, interact, if the normal overlap $\delta = 2R - |\underline{r}_i - \underline{r}_j|$ is positive. The *normal contact force* involves a linear repulsive and a linear dissipative force,

$$f_{ij}^n = k_n \delta + \gamma_n \, v_{ij}^n \,, \tag{3}$$

with normal spring stiffness k_n, normal viscous damping γ_n and normal velocity $v_{ij}^n = \dot{\delta}$. For the sake of brevity we did set rolling and torsion interactions to zero and focus on friction only, i.e. the *tangential friction force* is

$$f_{ij}^t = k_t \chi + \gamma_t \, v_{ij}^t \,, \tag{4}$$

with tangential spring stiffness k_t, tangential viscous damping γ_t and tangential velocity v_{ij}^t, where χ is the integral of v_{ij}^t over time, adapted such that the tangential force is limited by Coulomb sliding friction (with Coulomb's coefficient of friction μ_C), see also [19]. Note, that f_{ij}^n and f_{ij}^t give only non-zero contributions to $\underline{f}_{ij}$, when the two particles overlap. Details of the *capillary force* $f_{ij,c}$, which is also active when two particles separate after a contact, are given in the next subsection.

3.2 Capillary forces

For wet granular materials with low mass ratios between liquid and dry granular material we expect that the grains are connected by individual capillary bridges. The relevant parameters liquid volume V_b, length $s = -\delta$ and equilibrium contact angle $\theta < 90^o$ of such a bridge are indicated in Fig. 2(right).

With these parameters, we approximate the inter-particle force $f_{ij,c}$ and the critical length s_{crit} of the capillary bridge according to the proposal of Willett et al. [20]:

$$f_{ij,c} = \frac{2\,\pi\,\gamma\,R\,\cos{(\theta)}}{1 + 1.05\hat{s} + 2.5\hat{s}^2} \qquad s_{crit} = R\,\left(1 + \frac{1}{2}\theta\right)\left[\left(\frac{V_b}{R^3}\right)^{\frac{1}{3}} + 0.1\,\left(\frac{V_b}{R^3}\right)^{\frac{2}{3}}\right]. \qquad (5)$$

with surface tension γ and dimensionless bridge length $\hat{s} = s\,\sqrt{R/V_b}$. Note, that $f_{ij,c}$ exists only during and past a contact between particle i and j, providing a non-zero contribution to $\underline{f}_{ij}$ until the total distance s between i and j rises above the critical bridge length $s > s_{crit}$. Then, the bridge ruptures and $f_{ij,c}$ becomes zero – until, possibly, the contact is re-established at $s_0 \approx 0$, but we ignore any liquid layer at the surface since $s_{crit} \gg s_0$.

The model equations presented above were implemented into the open-source DEM software package LIGGGHTS, version 2.3.2. The simulations were carried out at the HPC cluster CVC at the University Computer Center of the TU Bergakademie Freiberg.
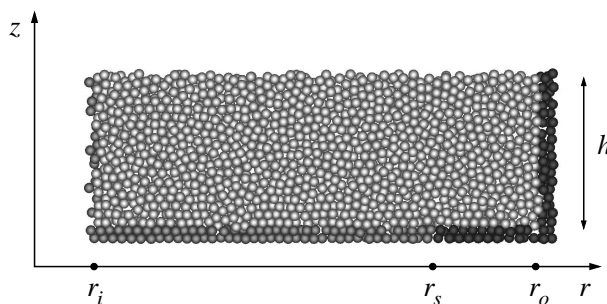
Figure 3: Setup of the numerical rheometer in cylindrical (r, z) coordinates; light gray: sheared granular material, medium gray: static, inner part of the shear cell, dark gray: rotating, outer part of the shear cell (the medium and dark gray particles are part of the rough walls of the shear cell and thus displayed as particles).

### 3.3 Setup of the numerical rheometer

The flow and rheology of wet granular materials in a three-dimensional split bottom shear cell [11, 16, 17, 18] are investigated with the DEM model. Basic parameters of the shear cell geometry are sketched in Fig. 3, with the values: $r_i = 14.7\,\mathrm{mm}$, $r_s = 85\,\mathrm{mm}$, $r_o = 110\,\mathrm{mm}$, and the shear velocity of the outer cylinder wall, $U_o = 6.9\,\mathrm{mm/s}$. The rheometer is filled with $n_P \simeq 210000$ particles, which all have the same diameter $d_P = 2\,\mathrm{mm}$, with density $\rho_P = 2000\,\mathrm{kg/m^3}$. The mechanical parameters of the particles are chosen as $k_n = 110\,\mathrm{N/m}$, $\gamma_n = 2 \cdot 10^{-3}\,\mathrm{kg/s}$, $k_t = 12\,\mathrm{N/m}$, $\gamma_t = 0.5 \cdot 10^{-3}\,\mathrm{kg/s}$, and $\mu_C = 0.01$.

Simulations with wet granular materials should reveal if the influence of the liquid bridges on the apparent shear viscosity is the same as in the experiments. For the simulations of wet granular materials, the equilibrium contact angle $\theta = 0°$ and the surface tension $\gamma = 20.6\,\mathrm{mN/m}$ were kept constant, while the dependence on those parameters was discussed in Ref. [15] and is examined further in ongoing research. The simulations were conducted for dry granular material and for two different bridge volumes V_b (4.2 nl, 42 nl) for each capillary bridge.

4   RESULTS

4.1   Particle kinematics

In the sheared granular material, the moving slit initiates a shear band that moves inwards and becomes wider with increasing height, see Fig. 4. The colors indicate the particle velocities v_p in tangential φ-direction and show that the liquid bridge volume V_b has a significant influence on the shear band structure.
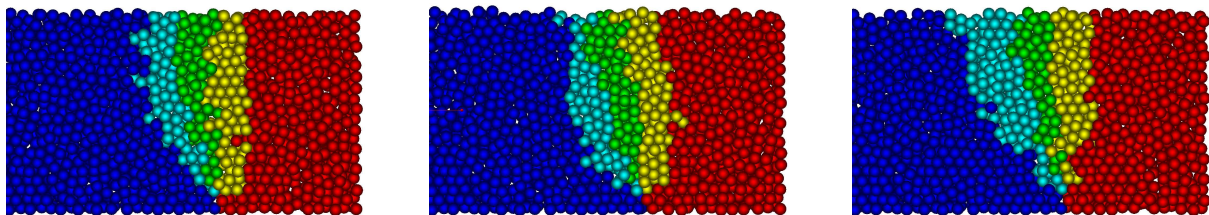
Figure 4: Snapshots from simulations with different liquid bridge volumes V_b, seen from (view in angular cylindrical direction, perpendicular to the r-z-plane). The granular material is (left) dry ($V_b = 0\,\mathrm{nl}$) and contains liquid bridges with (middle) $V_b = 4.2\,\mathrm{nl}$ and (right) $V_b = 42\,\mathrm{nl}$. The colors from the center outwards denote particles with particle velocities in tangential direction of around $v_p = 0.1$ mm/s (blue), $v_p = 1.4$ mm/s (light blue), $v_p = 2.9$ mm/s (green), $v_p = 4.4$ mm/s (yellow), and $v_p = 6.8$ mm/s (red).

4.2   Averaging and micro-macro transition

Since translational invariance in the tangential φ-direction is assumed, pure averaging is performed over ring-shaped volumes ΔV at various positions $\underline{r} = (r, z)$ in the system

(with cylindrical coordinates) and over many snapshots in time (typically 50 ... 100), leading to fields $Q(r, z)$ of the averaged quantities. As an example, the average number of mechanical contacts $n(r, z)$ (with $\delta \geq 0$) and pure wet contacts $n_w(r, z)$ (with $\delta < 0$ and $s < s_{crit}$ after a mechanical contact) of the particles are given in Fig. 5. As expected, the average number of mechanical contacts is typically in the range $6.5 \lesssim n \lesssim 7$, whereas the number of pure wet contacts is in a significantly lower range $0.2 \lesssim n_w \lesssim 0.7$. The purely wet contacts, quantified via n_w, have a more visible dependence on both r and z than the mechanical contacts, quantified by n. For the mechanical contacts, only at a few positions, they exceed 7, close to the bottom inside the shearband. Values of n smaller than 6.5 are observed at a few (random) positions and at the surface. In conctrast, n_w values are clearly largest in the center of the shear band where the shear rate is largest, and become extremely large close to the free surface, where the pressure is lowest. These interesting height- and shear-rate-dependencies require further study.

As in Refs. [16, 17, 18], continuum quantities like the solid-fraction ϕ, the velocity-field $\underline{u}$ or the stress-field $\underline{\underline{\sigma}}$ are computed by a micro-macro transition method from the DEM results, e.g.,

$$\phi(\underline{r}) = \frac{1}{\Delta t \, \Delta V} \int_{\Delta t} \sum_{i \in \Delta V} V_i \, dt \,, \tag{6}$$

$$\underline{u}(\underline{r}) = \frac{1}{\Delta t \, \Delta V} \int_{\Delta t} \left(\sum_{i \in \Delta V} V_i \, \underline{v}_i \right) dt \times \frac{1}{\phi(\underline{r})} \,, \tag{7}$$

$$\underline{\underline{\sigma}}(\underline{r}) = \frac{1}{\Delta t \, \Delta V} \int_{\Delta t} \left(\sum_{i \in \Delta V} m_i \underline{v}'_i \otimes \underline{v}'_i + \sum_{c \in \Delta V}^{\{i,j\}=c} \underline{f}_{ij} \otimes \underline{l}_{ij} \right) dt \,, \tag{8}$$

with fluctuation velocity $\underline{v}'_i = \underline{v}_i - \underline{u}(\underline{r})$, using averaging time intervals of typically $\Delta t = 5\,\mathrm{s}$, a discrete averaging time-step $dt = 0.05\,\mathrm{s}$, and particle volume V_i. Further scalar fields like strain rate magnitude, shear stress magnitude, hydrostatic pressure and apparent viscosity can be calculated from the tensor fields as:
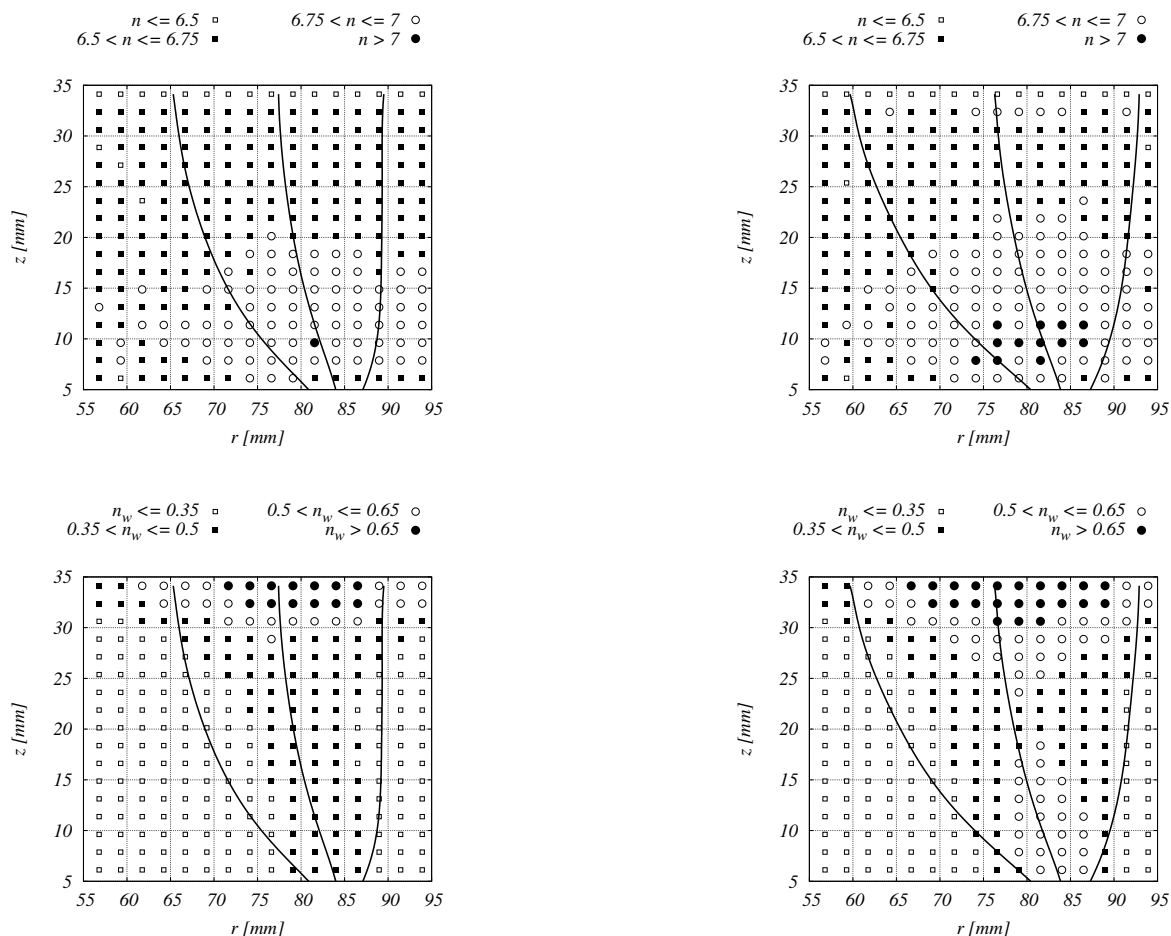
$$\dot{\gamma} = \frac{1}{2} \sqrt{\left(\frac{\partial u_\varphi}{\partial r} - \frac{u_\varphi}{r} \right)^2 + \left(\frac{\partial u_\varphi}{\partial z} \right)^2} \,, \tag{9}$$

$$|\tau| = \sqrt{\sigma_{r\varphi}^2 + \sigma_{z\varphi}^2} \,, \tag{10}$$

$$p = \frac{1}{3} \left(\sigma_{rr} + \sigma_{zz} + \sigma_{\varphi\varphi} \right) \,, \tag{11}$$

$$\eta = \frac{|\tau|}{\dot{\gamma}} \,, \tag{12}$$

In contrast to the experimental setup, the macroscopic fields from simulations can be investigated *locally*, i.e., at arbitrary positions $\underline{r}$ anywhere in the filled measurement volume

Figure 5: Average number of (first row) mechanical contacts n and (second row) pure wet contacts n_w from the DEM simulations. The wet material contains liquid bridges with (left column) $V_b = 4.2\,\text{nl}$ and (right column) $V_b = 42\,\text{nl}$. The solid lines indicate the shear band center and half-widths.

(gap) of the rheometer. Furthermore, a lot of microscopic information (see n and n_w) is available that cannot be obtained from most experiments.

All simulations discussed below run for 20 s. For the average, only the period between 15 s and 20 s is taken into account. Therefore, the system is examined in quasi-steady state flow conditions (the transient behavior at the onset of shear is disregarded). However, it cannot be excluded, that long-time relaxation effects may have an influence on our findings, which is not adequately resolved by our relatively short simulations.

4.3 Local shear viscosities

The local shear viscosities η for dry and different wet granular materials within the shear band are compared in Figs. 6 and 7. The viscosity fields $\eta(r, z)$ in the dry and wet granular material differ markedly, see Fig. 6. Similar to the experiments, the inverse

8
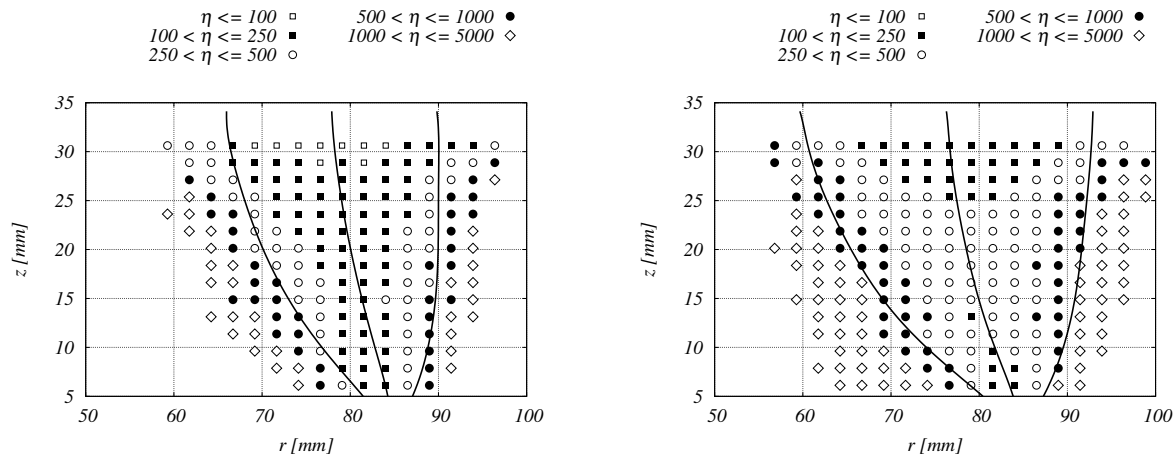
Figure 6: Local shear viscosity $\eta(r, z)$ (in units of [Pa s]) from the DEM simulations with (left) dry material and (right) wet material (liquid bridges with $V_b = 42$ nl) in the sheared region (local strain rate $\dot{\gamma} \geq 0.01\,\mathrm{s}^{-1}$). The solid lines indicate the shear band center and half-widths.

proportional dependence of the apparent viscosity on (in this case) the inertial number I is evidenced for the dry and wet material, and, as to be expected, the addition of small amounts of liquid increases the viscosity by about 10 to 20%, see Fig. 7. The inset with linear axes gives an exemplary illustration, (the change appears not that large only due to the logarithmic vertical axis in the global plots). The scaling $\eta \sim I^{-\alpha}$ changes from $\alpha = 0.9$ to $\alpha = 2$ in all materials, in different regimes, see Ref. [15]. For the sake of clarity, in Fig. 7 only data points with pressure levels $p > 200\,\mathrm{Pa}$ are shown following the $\alpha = 0.9$ trend. Only data points with lower pressure levels display the second branch with scaling $\alpha = 2$, which is also shifted towards higher viscosities for wet granular materials (data not shown here).

5 CONCLUSIONS

Weakly wetted granular materials are examined in shear experiments and by corresponding numerical rheometer studies using DEM simulations. Rheological data from the experiments and the simulations show reasonable agreement, so that the numerical results can now be used to gain a better understanding of the flow rules and their microscopic origin, with – in future – to apply those in CFD macro-simulations of wet granular media.

A shear-thinning behavior of the granular material is found with both approaches. Additionally, the local shear viscosity of the granular material in the DEM simulations significantly increases when only small amounts of liquid are added to the material, representing well the trend as seen for the apparent global shear viscosity from the experiments.

Furthermore, the DEM simulations of wet granular material show that the internal structure of the sheared material (i.e., the shear bands) are qualitatively the same as for dry materials. However, the liquid content influences shear bands in a non-trivial
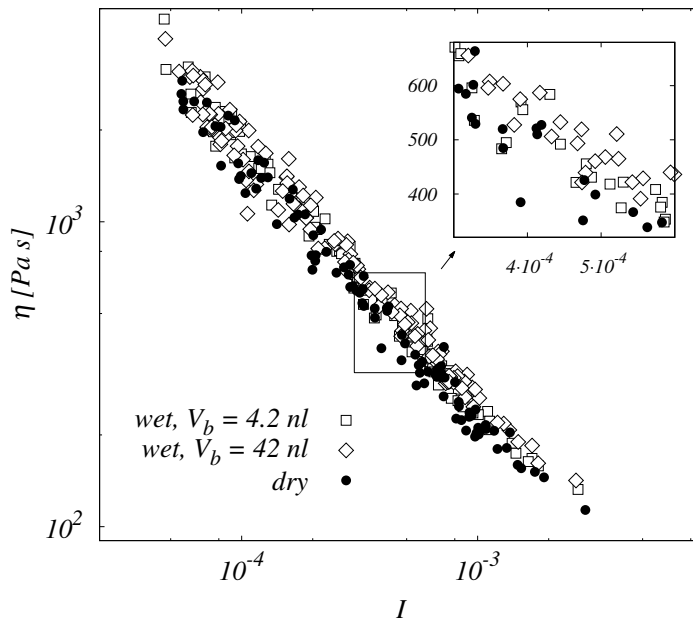
Figure 7: Local shear viscosity $\eta(I)$ from the DEM simulations from data with $p > 200\,\mathrm{Pa}$. Different symbols indicate results from dry ($\bullet$) and wet material (open symbols). The wet material contains liquid bridges with $V_b = 4.2\,\mathrm{nl}$ ($\square$) and (bottom) $V_b = 42\,\mathrm{nl}$ ($\diamond$).

manner. A little bit of liquid seems to narrow the shear band while more liquid content added leads to wider shear bands. Interestingly, there are more purely wet "contacts", i.e. liquid bridges without mechanical contacts, in the center of the shear band (which can be expected due to the tensile mode of deformation in one direction inside the shear plane), but also closer to the surface, where the confining pressure is smallest.

The influence of other wetting parameters (e.g. contact angle) on the rheology of the wet granular materials is presently investigated in more detail and results will be published elsewhere. Future studies should also involve better micro-models (with e.g. a possible re-distribution of liquid during shear [7]), and a more quantitative study of the constitutive relations that describe the rheology of the material and their microscopic origin.

ACKNOWLEDGMENTS

REFERENCES

[1] GDR Midi. On dense granular flows. *Eur. Phys. J. E* (2004) **14**:341–365.

[2] Forterre, Y. and Pouliquen, O. Flows of dense granular media. *Ann. Rev. Fluid Mech.* (2008) **40**:1–24.

[3] Iveson, S.M. Nucleation, growth and breakage phenomena in agitated wet granulation processes: a review. *Pow. Tech.* (2001) **117**:3–39.

[4] Beeley, P.R. *Foundry technology.* Elsevier Butterworth-Heinemann, Oxford (2001)

[5] Tardos, G.I., McNamara, S., Talu, I. Slow and intermediate flow of a frictional bulk powder in the Couette geometry. *Pow. Tech.* (2003) **131**:23–39.

[6] Herminghaus, S. Dynamics of wet granular matter. *Adv. Phys.* (2005) **54**:221–261.

[7] Mani, R., Kadau, D., Herrmann, H.J. Fluid depletion in shear bands. *Phys. Rev. Lett.* (2012) **109**:248001.

[8] Schwarze, R., Rudert, A., Tilch, W. and Bast, J. Rheological behavior of sand-binder mixtures measured by a coaxial cylinder rheometer. *I. Foundry Res.* (2008) **60**(3):2–6.

[9] Liao, C.-C. and Hsiau, S.-S. Experimental analysis of dynamic properties in wet sheared granular matter. *Pow. Tech.* (2010) **197**:222-229.

[10] Rudert, A., Schwarze, R., Tilch, W. and Bast, J. Computational fluid dynamics of the core shooting process. *Foundry Trade J. I.* (2011) **185**:147–151.

[11] Fenistein, D., van de Meent, J.W. and van Hecke, M. Universal and wide shear zones in granular bulk flow. *Phys. Rev. Lett.* (2004) **92**:094301.

[12] McCarthy, J.J. Micro-modeling of cohesive mixing processes. *Pow. Tech.* (2003) **138**:63–67.

[13] Anand, A., Curtis, J.S., Wassgren, C.R., Hancock, B.C. and Ketterhagen, W.R. Segregation of cohesive granular materials during discharge from a rectangular hopper. *Gran. Mat.* (2010) **12**:193–200.

[14] Radl, S., Kalvoda, E., Glasser, B.J. and Khinast, J.G. Mixing characteristics of wet granular matter in a bladed mixer. *Pow. Tech.* (2010) **200**:171–189.

[15] Schwarze, R., Gladkyy, A., Uhlig, F. and Luding, S. Rheology of weakly wet granular materials a comparison of experimental and numerical data. *Gran. Mat.* (2013) **15** (in press).

[16] Luding, S. The effect of friction on wide shear bands. *Part. Sci. Technol.* (2008) **26**:33–42.

[17] Luding, S. Constitutive relations for the shear band evolution in granular matter under large strain. *Particuology* (2008) **6**:501–505.

[18] Luding, S. and Alonso-Marroquin, F. The critical-state yield stress (termination locus) of adhesive powders from a single numerical experiment. *Gran. Mat.* (2011) **13**:109–119.

[19] Luding, S. Cohesive frictional powders: Contact models for tension. *Gran. Mat.* (2008) **10**:235–246.

[20] Willett, C.D., Adams, M.J., Johnson, S.A. and Seville, J.P.K. Capillary bridges between two spherical bodies. *Langmuir* (2000) **16**:9396–9405.